REGULAR ARTICLE

blood advances

Novel GNE missense variants impair de novo sialylation and cause defective angiogenesis in the developing brain in mice

Lulu Huang,[1,2,*] Yuji Kondo,[3,*] Lijuan Cao,[1] Jingjing Han,[1] Tianyi Li,[1] Bin Zuo,[1] Fei Yang,[1] Yun Li,[1] Zhenni Ma,[1] Xia Bai,[1,2,4] Miao Jiang,[1] Changgeng Ruan,[1,2,4] and Lijun Xia[1,2,5]

[1]Jiangsu Institute of Hematology, National Clinical Research Center for Hematologic Diseases, NHC Key Laboratory of Thrombosis and Hemostasis, The First Affiliated Hospital of Soochow University, Suzhou, China; [2]Collaborative Innovation Center of Hematology, and [4]State Key Laboratory of Radiation Medicine and Protection, Soochow University, Suzhou, China; [3]Institute for Glyco-core Research, Nagoya University, Nagoya, Japan; and [5]Cardiovascular Biology Research Program, Oklahoma Medical Research Foundation, Oklahoma City, OK

Key Points

- A pediatric patient presented with macrothrombocytopenia carrying 2 novel *GNE* missense variants (C594Y and P735R).
- Mice with homozygous P735R mutations exhibited defective angiogenesis and cerebral hemorrhages as early as E11.

Glucosamine (UDP-N-acetyl)-2-epimerase and N-acetylmannosamine (ManNAc) kinase (GNE) is a cytosolic enzyme in de novo sialic acid biosynthesis. Congenital deficiency of GNE causes an autosomal recessive genetic disorder associated with hereditary inclusion body myopathy and macrothrombocytopenia. Here, we report a pediatric patient with severe macrothrombocytopenia carrying 2 novel *GNE* missense variants, c.1781G>A (p.Cys594Tyr, hereafter, C594Y) and c.2204C>G (p.Pro735Arg, hereafter, P735R). To investigate the biological significance of these variants in vivo, we generated a mouse model carrying the P735R mutation. Mice with homozygous P735R mutations exhibited cerebral hemorrhages as early as embryonic day 11 (E11), which subsequently progressed to large hemorrhages in the brain and spinal cord, and died between E11.5 and E12.5. Defective angiogenesis such as distended vascular sprouts were found in neural tissues and embryonic megakaryocytes were abnormally accumulated in the perineural vascular plexus in mutant mouse embryos. Furthermore, our in vitro experiments indicated that both C594Y and P735R are loss-of-function mutations with respect to de novo sialic acid biosynthesis. Overall, this study reveals a novel role for GNE-mediated de novo sialic acid biosynthesis in mouse embryonic angiogenesis.

Introduction

Sialic acid is a common capping structure on nonreducing terminus of glycans on proteins and lipids, a biochemical process named sialylation. Because of its negative charge, sialic acid imparts an electrostatic repulsive force to glycans. Sialic acid also interacts with many sialic acid binding proteins such as sialic acid binding immunoglobulin-like lectins. As a result, sialylation has critical biological functions, especially in cell-cell interactions.[1,2] Sialylation takes place in the Golgi. There are 2 pathways to synthesize the sialic acid precursor for sialylation. One is glucosamine-2-epimerase and N-acetylmannosamine kinase (GNE)–mediated de novo sialic acid biosynthesis, and the other results from lysosomal degradation of glycoconjugates by lysosomal neuraminidase.[3]

Submitted 21 August 2023; accepted 10 January 2024; prepublished online on *Blood Advances* First Edition 18 January 2024; final version published online 16 February 2024. https://doi.org/10.1182/bloodadvances.2023011490.

*L.H. and Y.K. are joint first authors.

All data will be available after publication.

Bulk RNA-sequencing data have been deposited to GneBank (Accession ID SAMN38929975, SAMN38929976, SAMN38929977, SAMN38929978, SAMN38929979, SAMN38929980, SAMN38929981, SAMN38929982, SAMN38929983, and SAMN38929984).

The full-text version of this article contains a data supplement.

GNE consists of 2 functionally distinct domains: UDP-GlcNAc-2-epimerase on the N-terminus and the ManNAc kinase on the C-terminus.[4] The former activity is required for the epimerization of UDP-GlcNAc to ManNAc, and the latter is for the following phosphorylation of ManNAc to ManNAc-6-phosphate. Then, ManNAc-6-phosphate is modified to sialic acid-9-phosphate and subsequently dephosphorylated to sialic acid, which is then converted to CMP-sialic acid in the nucleus. CMP-sialic acid is transported to the Golgi apparatus by the specific CMP-sialic acid transporter Slc35a1 for sialylation of glycans.[5] To prevent overproduction of sialic acid, GNE is allosterically inhibited by CMP-sialic acid.[6]

Congenital deficiency of *GNE* causes an autosomal recessive genetic disorder. Different *GNE* mutations in humans cause 2 distinct phenotypes; sialuria, a disorder of sialic acid metabolism, and hereditary inclusion body myopathy (HIBM).[7] The former is inherited as an autosomal dominant trait and presents as sialic acid overproduction due to impaired allosteric inhibition mechanism.[6,8] The latter is an adult-onset autosomal recessive disorder, and the pathological mechanism still remains unclear.[9] One proposed mechanism of HIBM is based on the lack of functional glycosylation of dystroglycan, a transmembrane protein that plays an important role in transducing extracellular matrix–derived signals to the cytoskeleton and provides physical strength to the skeletal muscle cell membrane.[10-12]

Since the first genomic mutation in *GNE* was discovered in a patient with sialuria in 1989,[13] several *GNE* variants have been reported to be relevant to sialuria and HIBM.[7,9,14] Sialuria is caused by *GNE* mutation–mediated impairment of the inhibitory feedback in the sialic acid production pathway and is inherited as an autosomal dominant trait, whereas loss-of-function *GNE* mutations cause HIBM as an autosomal recessive disease. Interestingly, several recent reports have shown that *GNE* pathogenic variants are associated with congenital macrothrombocytopenia and, in some cases, with concomitant myopathy.[15-18] Some studies have suggested that impaired sialylation of platelet surface glycans leads to shorter platelet lifespan,[18,19] thereby contributing to GNE-associated macrothrombocytopenia. However, the exact mechanism of GNE-related diseases is not yet fully understood.

In this study, we report on a pediatric patient with severe macrothrombocytopenia. Next-generation sequencing technology identified compound heterozygous *GNE* variants in the patient, c.1781G>A (C594Y) and c.2204C>G (P735R). To investigate the pathological significance of these variants, we generated a new mouse model carrying a homozygous P735R missense mutation. Unexpectedly, P735R homozygous embryos exhibited cerebrospinal hemorrhages at embryonic day 11 (E11) and became nonviable between E11.5 and E12.5. Defective angiogenesis, such as abnormal vascular sprouts in neural tissues budding from the perineural vascular plexus, was discovered in the diencephalon at E11 in the mutant (mt) mice. After the in vivo work, we analyzed these patient-derived variants by establishing *Gne*-knockout (KO) mouse endothelial cell line, MS1 cells transduced with human GNE carrying C594Y or P735R using lentiviral vectors, and discovered that both C594Y and P735R are loss-of-function mutations. Altogether, our studies reveal novel *GNE* pathogenic variants that contribute to macrothrombocytopenia in human and provide new insights into GNE-mediated de novo sialic acid biosynthesis during embryonic vascular development in mice.

Material and methods

Study design

The study design was focused on the functional characterization of novel pathogenic variants in *GNE* of a patient with macrothrombocytopenia we identified. This includes in vitro approaches, such as mouse endothelial MILE SVEN 1 (MS1) cells transfected with the *GNE* variants, and a newly generated knockin mouse model carrying one of the pathogenic variants in *GNE* to determine the pathogenic roles of the *GNE* variant. Both the patient and mouse studies were approved by the institutional review boards and the Animal Use Committee of the First Affiliated Hospital of Soochow University.

Generation of *Gne*$^{+/P735R}$ mice

To generate a C57BL/6J mouse background with a point mutation (c.2204C>G, P735R) at the mouse *Gne* locus, a gRNA targeting vector and donor oligo (with 9 bp targeting sequence, flanked by 60 bp homologous sequences on both sides) were designed. The P735R (CCG to CGG) and a synonymous mutation p.Leu737 (CTG to TTA) were introduced into exon 12. After obtaining mt mice, the pups were genotyped by PCR, followed by sequence analysis, and heterozygotes were kept for breeding. To eliminate off-target effects, heterozygous founder mice were backcrossed with wild-type (wt) mice for at least 3 generations. In each breeding generation, breeders were selected by specific genotyping of the targeted knockin mutation. All mice were housed in humidity- and temperature-controlled specific pathogen-free animal facilities on a 12 hour light-dark cycle with free access to food and water. Timed-mated females were obtained from natural matings by crossing males with females of breeding age. The presence of a copulatory plug denoted E0.5.

Animal studies were conducted under protocols approved by the Institutional Animal Care and Use Committee of Soochow University. The human study was approved by the Ethics Committee of the First Affiliated Hospital of Soochow University. Written informed consent was obtained from the parent of the patient before enrollment.

Histology, immunostaining, and image acquisition

Mouse embryos were collected and photographed at dissection. For histology, embryos were fixed in 10% formalin, and 5-μm paraffin-embedded coronal sections were cut and stained with hematoxylin and eosin. For immunofluorescence, tissues were fixed in 4% paraformaldehyde, and cryosections were cut at a thickness of 20 to 50 μm, blocked, incubated with primary and then secondary antibodies, counterstained with nuclear marker, and mounted for imaging with a Leica TCSSP8 microscope system.

Data analysis and statistics

Statistical tests were performed using Prism software (GraphPad, San Diego, CA). Two-sided Student *t* tests were performed to assess the statistical significance of differences between 2 groups after confirming that the data met the criteria of normal distribution and equal variance. Differences were considered statistically significant when $P < .05$.

Additional methods can be found in the supplemental Information.

Results

Novel missense mutations in *GNE* gene were identified in a patient with macrothrombocytopenia

The patient had continuous epistaxis starting at the age 5. His blood tests and bone marrow examination revealed a low platelet count <20 000 cells/μL with no other abnormalities, and the bone marrow aspirate smear showed megakaryocytes of normal number and size. He was diagnosed with immune thrombocytopenia and has been treated with glucocorticoid, IV immunoglobulin, cyclosporine, danazol, and eltrombopag since at local hospitals. However, his platelet count remained at 10 000 to 30 000 cells/μL. At age 13, he was admitted to the First Affiliated Hospital of Soochow University. On physical examination, the patient was found to have purpura and asthenia. He also had growth retardation with a height of 140 cm, which is less than −2 standard deviation of the height of general population, based on the Standard Deviations of Height and Weight for Children and Adolescents Aged 0 to 18 years in China.[20] However, he had no pain, sensory disturbance, muscle cramps, or other signs of myopathy, and no marked weakness of cardiopulmonary function, along with normal spleen size and serum creatine kinase concentration. Besides, he had no other medical complications, and none of his family members had similar symptoms.

Blood tests revealed that his platelet count was 28 000 cells/μL as shown in supplemental Table 1, and the peripheral blood smear displayed markedly enlarged platelets compared with normal platelets (Figure 1A). Targeted exome sequencing using a 199-gene panel for congenital bleeding disorders (supplemental Table 2) was performed and we identified 2 heterozygous missense variants in the *GNE* gene, c.1781G>A (NM_001128227.3: C594Y) in exon 10 and c.2204C>G (NM_001128227.3: P735R) in exon 12, whereas no other mutation was found. Further Sanger sequencing of *GNE* confirmed these 2 mutations in the patient, and his father has the same c.1781G>A heterozygous mutation (Figure 1B). Because his mother's DNA sample was not available, it is presumed that the c.2204C>G mutation was inherited from his mother (Figure 1C). Most of patients with *GNE* mutations have either 1 homozygous missense variant or 2 heterozygous missense variants; one on the epimerase domain and the other on the kinase domain, respectively.[7] Therefore, it is rare for the 2 heterozygous mutations to be located on the C-terminal ManNAc kinase domain, as in our patient (Figure 1D).

Because GNE is required for de novo sialic acid biosynthesis and sialic acid on platelets is a determinant of platelet's lifespan,[17,21] the thrombocytopenia in this patient could be the result of altered glycans on the platelet surface. To test this, platelets from the family members were isolated and analyzed by flow cytometry. To lessen the effect of the giant size of the patient's platelets on the mean fluorescence intensity (MFI), we divided the MFI with the forward scatter (FSC) as the normalized MFI. The normalized MFI of CD42a, a platelet marker, and MAL-II, which detects α2,3-linked sialic acids, were decreased in the patient's platelets compared

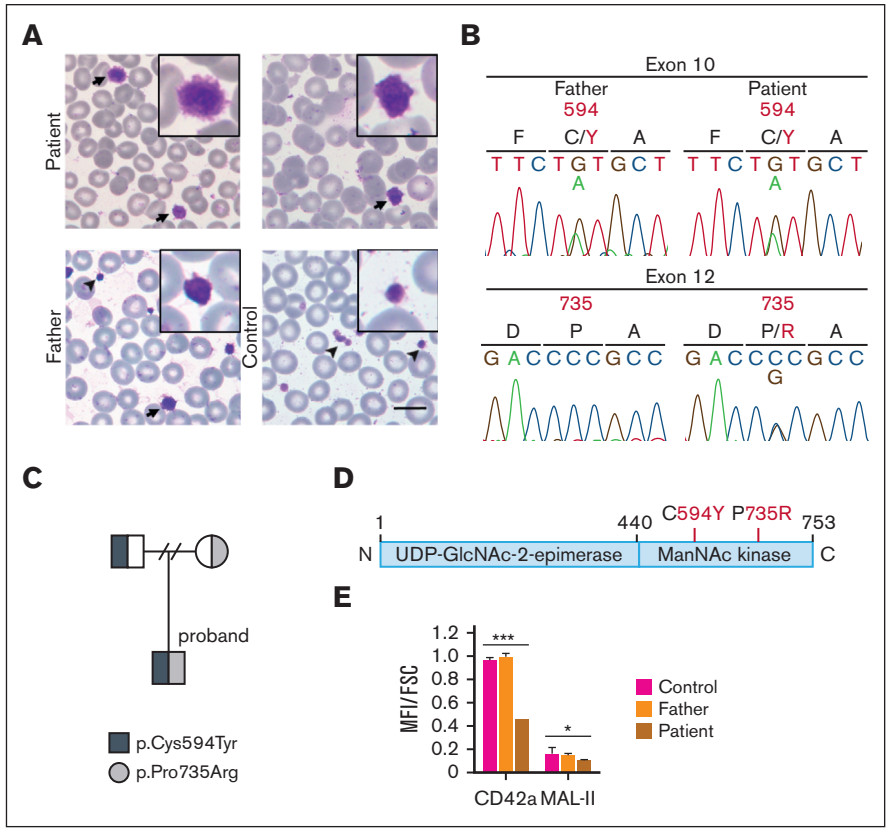

Figure 1. Identification of *GNE* compound heterozygote variants in a patient with macrothrombocytopenia. (A) Representative images of Giemsa staining of peripheral blood smears from the patient (age 16), the patient's father (age 40), and a healthy individual (age 28) as normal control who has no family relationship with the patient or his other family members. The size of patient's platelets was nearly 3 times larger than that of the normal control. Arrows indicate enlarged platelets. Arrowheads indicate normal platelets. Black boxes indicate platelets with higher magnification. Scale bar, 10 μm. (B) Genomic DNA sequences of exon 10 and exon 12 of *GNE* in father- and patient-derived blood cells. Letters and numbers in red indicate mutated residues and sites in the GNE protein sequence, respectively. (C) Pedigree of the family. The filled square indicates the patient, who is the proband, and the half-filled square and circle indicate heterozygous father and mother, respectively. (D) Schematic domain structure of GNE carrying combined missense mutations in the patient. (E) MFI of MAL-II and platelet surface marker CD42a on peripheral platelets from the patient, patient's father and a healthy individual as normal control (the same individual as in Figure 1A), respectively. MFI, mean fluorescence intensity; FSC, forward scatter; MAL-II, Maackia amurensis lectin II, binds to α-2,3 linked sialic acid. *$P < .05$; ***$P < .001$.

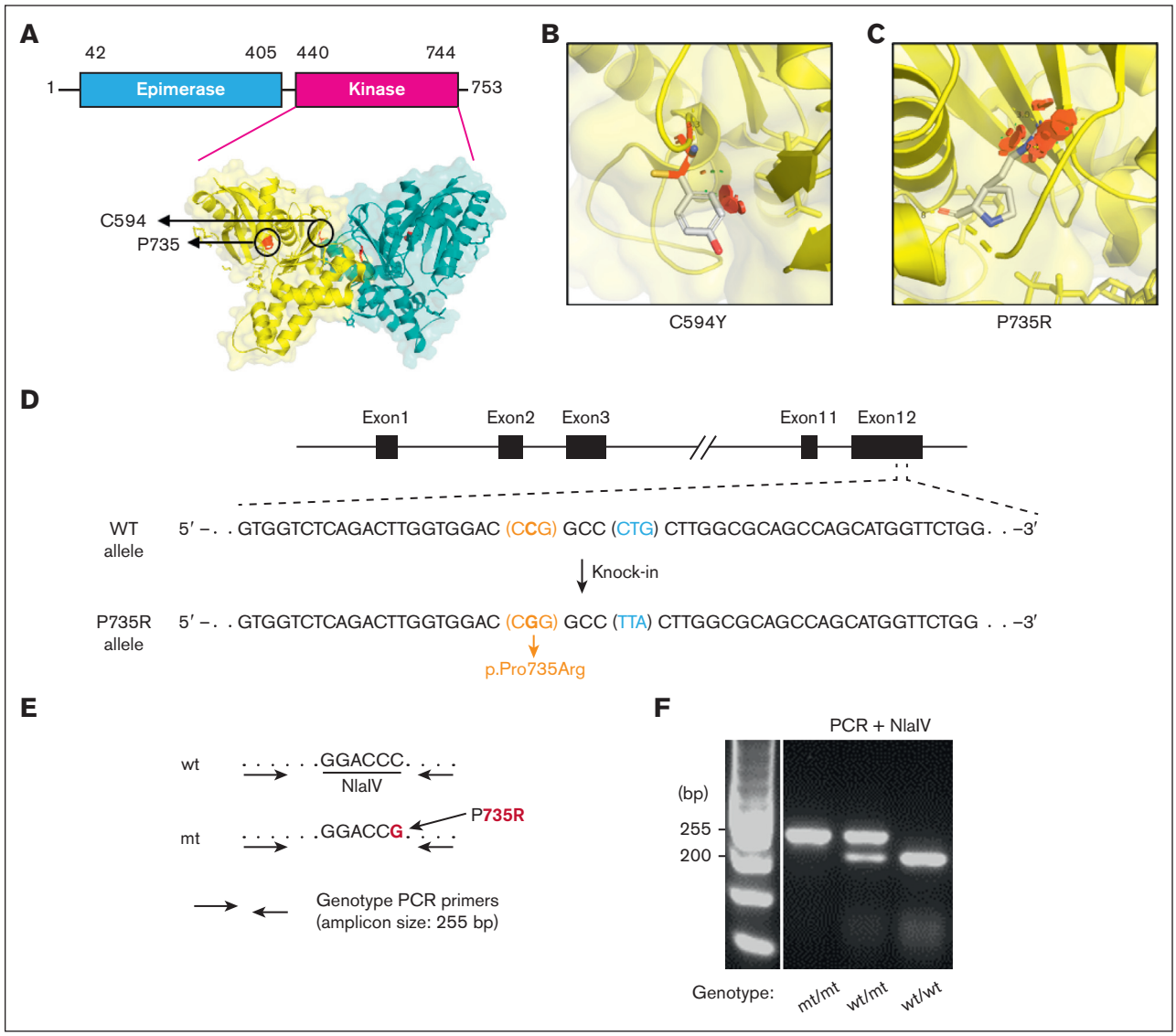

Figure 2. Generation of P735R-knockin mice. (A) Schematic domain representation of UDP-GlcNAc-2-epimerase and ManNAc kinase in human GNE, and the structure of dimeric kinase domains (PDB ID: 2YHW). (B) Structural prediction of kinase domain carrying C594Y mutation, showing that 1 rotamer causes severe clashes in all 3 rotamers. (C) Structural prediction of kinase domain carrying P735R mutation, showing severe clashes for all the 22 rotamers. Mutagenesis and rotamer selection were performed using PyMOL, in which the gray sticks indicate the mutated residues and the red octagon disks indicate significant van der Waals overlap, meaning atoms are close to other atoms causing clashes. (D) Diagram of the targeted genomic sequence in the *Gne*$^{P735R/P735R}$ (hereafter, mt/mt) mouse using the CRISPR-Cas9 system. The synonymous mutation p.Leu737 (CTG to TTA) was introduced as a blocking mutation to prevent re-cutting by Cas9 after homology-directed repair. (E) Illustration of the RFLP-based genotyping assay using PCR and restriction endonuclease NlaIV. (F) Genotyping results visualized using 2% agarose/TBE gel.

with those of his father (Figure 1E). This phenotypic characterization of platelet glycans suggests that thrombocytopenia in this patient is caused by a shorter platelet lifespan based on altered glycans, possibly sialylation.

Generation of a mouse model carrying the P735R mutation

We performed computational model simulations of the mutated protein structure. C594Y has 3 rotamers, one of which causes severe clash, whereas P735R has 22 rotamers, all of which cause severe clashes (Figure 2A-C). Hence, these results demonstrate that both of C594Y and P735R could be pathological. Analysis of the primary sequence of GNE also revealed that exon 12 containing p.Pro735 is more conserved across several species than that around p.Cys594 (supplemental Figure 1A, B). Therefore, to investigate the pathogenicity of these mutants in vivo, we chose to generate a mouse model in the C57BL/6J background carrying a c.2204C>G (P735R missense mutation) via CRISPR-Cas9-mediated genome editing (Figure 2D). To this end, we designed a dual-sgRNAs expression vector targeting exon 12 and a 129-bp donor oligo in which the targeting 9-bp sequence was flanked by 60-bp homologous sequences. The missense mutation P735R (CCG to CGG) in the donor oligo was introduced into exon 12 in

the genome of fertilized eggs by homology-directed repair. In addition, a synonymous mutation p.Leu737 (CTG to TTA) was introduced as a blocking mutation to prevent sgRNAs from binding and recutting the sequence by Cas9 after successful homology-directed repair (Figure 2D). To genotype the mt pups, we developed a restriction fragment length polymorphism–based assay using PCR and the restriction endonuclease NlaIV, which cuts wt but not mt amplicons (Figure 2E,F).

Homozygous P735R mutants exhibit fatal cerebral hemorrhage at early embryonic stage

Heterozygous *Gne*$^{+/P735R}$ (hereafter, wt/mt) mice developed normally, of which both sexes appeared healthy with a normal life span. Similar to *Gne*$^{+/+}$ (hereafter, wt/wt) mice, wt/mt mice showed normal peripheral blood cell counts (supplemental Figure 2A,B). wt/mt mice were crossed to generate homozygous *Gne*$^{P735R/P735R}$ (hereafter, mt/mt) mice. A total of 395 viable pups were generated, of which 201 (51%) were male and 194 (49%) were female. Genotyping results showed that 134 (34%) were wt/wt, and 261 (66%) were wt/mt. However, no mt/mt genotype was identified among 395 viable pups. To determine whether P735R homozygosity causes embryonic lethality, we analyzed 313 embryos at E9.5 to E16.5 from timed matings by crossing wt/mt mice. Genotyping revealed 70 wt/wt (22.4%), 169 wt/mt (54%), and 74 mt/mt progenies (23.6%) as shown in supplemental Table 3.

At E11, mt/mt embryos appeared developmentally normal, but thereafter progressively developed large hemorrhages in the brain and spinal cord, whereas littermate wt/wt and wt/mt controls developed normally (Figure 3A). Embryonic hemorrhage consistently preceded death, supporting a causal relationship. Through observing heartbeat activity, 70.6% of mt/mt embryos died around E11.5, and all mt/mt embryos succumbed by E12.5. These results indicate that the P735R mutation causes a vital loss of GNE function.

Histology showed that the brains of mt/mt embryos exhibited bleeding into the third ventricle from the diencephalon at this stage of development (Figure 3B,C). There were fewer vascular sprouts

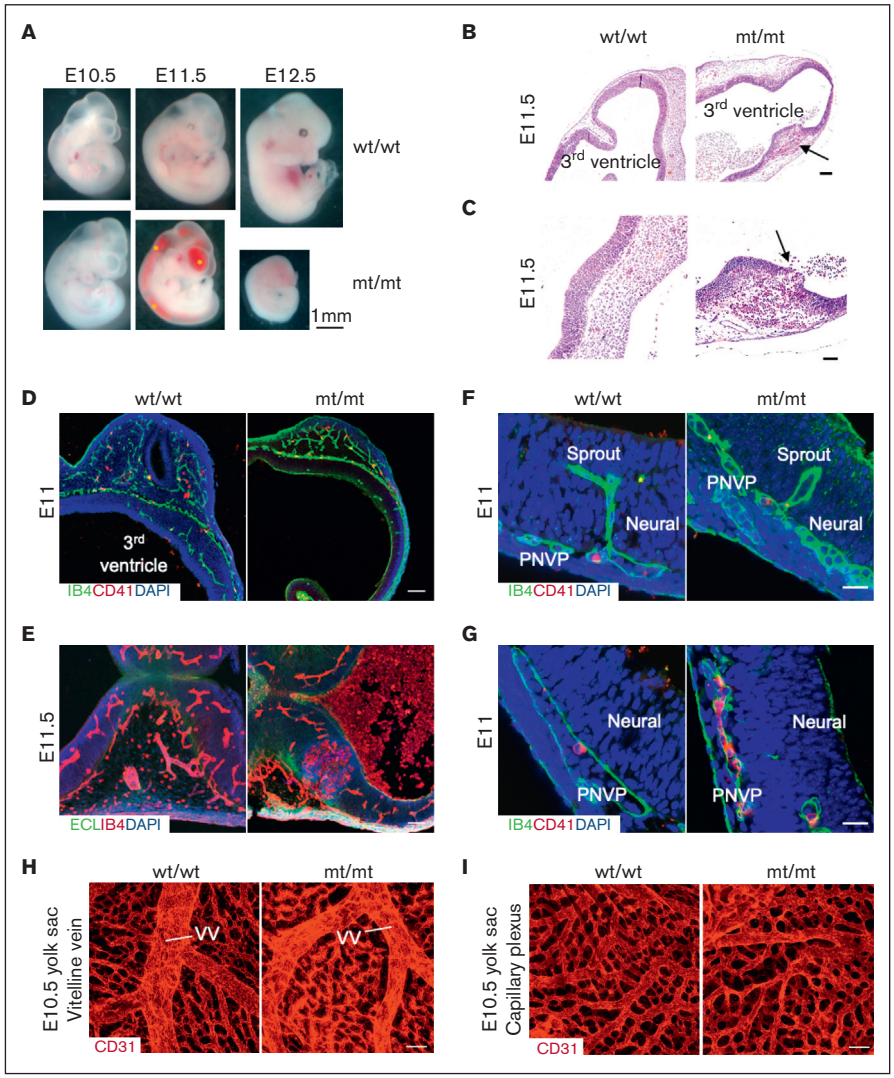

Figure 3. Homozygous P735R-knockin embryos develop distended vascular sprouts and spontaneous hemorrhages in the brain.
(A) Comparison of wt/wt and mt/mt embryos at different developmental stages. Blood is visible in the hearts of the older embryos. Asterisks indicate hemorrhages in the brain ventricles, spinal cord, and spinal canal of E11.5 mt/mt embryos. The E11.5 and E12.5 mt/mt embryos are dead and appear pale as blood circulation has ceased. (B) Hematoxylin-eosin staining of coronal section of the wt/wt and mt/mt embryos' heads at E11.5. Arrows indicate hemorrhagic lesions, which are shown at higher magnification in (C). Hemorrhages are visible in both the brain parenchyma as well as in the ventricles. Erythrocytes are nucleated at this stage of development. (D) Confocal images of angiogenic sprouting into the ventricle from PNVP of the diencephalon (coronal section) of E11 and (E) E11.5 embryos. (F) Confocal images of diencephalon distended sprouts and (G) accumulated eMKs in mt/mt embryos at E11. Neural, brain tissue. PNVP, perineural vascular plexus. ECL intensity reflects the degree of asialylation. In E11.5 mt/mt embryos, the hemorrhage penetrated the brain tissue and spread into the ventricle. IB4 marks the vasculature. CD41 marks eMKs and platelets (mostly eMKs at this stage). (H) Confocal microscopy images of wholemount stained E10.5 yolk sac with CD31 near the vitelline vein and (I) capillary plexus. Scale bar, 100 μm (B, D, F, H, I); 25 μm (C, E, G).

in neural tissues extending from the perineural vascular plexus in mt/mt embryos (Figure 3D). Moreover, there were distended and dilated sprouts in neural tissues at an early stage before the bleeding phenotype (Figure 3E,F; supplemental Figure 3A), suggesting that ruptured dilated vascular sprouts were most likely the source of hemorrhage. Spontaneous hemorrhages then occurred in the diencephalon or midbrain and developed into the ventricles by E11.5 (Figure 3B). Based on previous studies, we hypothesized that the homozygous *Gne* P735R mutation affects embryonic megakaryocytes (eMKs) and platelets through hyposialylation of mucin-type *O*-glycosylation of proteins such as podoplanin.[22] Supporting this hypothesis, quantification results of immunofluorescence staining displayed that the number of circulating platelets, eMKs and vascular sprouts emerging from perineural vascular plexus were significantly decreased in mt/mt embryos compared with wt/wt mice (Figure 3G; supplemental Figure 3B). Besides, no obvious morphological abnormalities of both vitelline vein and capillary plexus were found in yolk sacs compared with wt/wt embryos (Figure 3H,I), suggesting that the impaired growth in mt/mt embryos was not the consequence of extrinsic yolk sac development.

Mutated GNE affects gene expression related to angiogenesis

To determine how the GNE mutant causes defective angiogenesis in the developing brain, we performed bulk RNA sequencing (RNA-seq) using E11.5 embryo heads (n = 5 in each group) (Figure 4A,B; supplemental Figure 4A,B). Principal component analysis revealed a global difference in gene expression profiles between mt/mt and wt/wt embryos. According to gene ontology (GO) analysis, P735R mutation mainly enriched pathways related to sugar metabolism, probably due to the limited bioavailability of sialic acid in mt/mt mice (supplemental Figure 4A). We performed enrichment analysis using Metascape and found that regulation angiogenesis was one of the most significant GO biological processes (supplemental Figure 5A-C). Besides, we performed the gene set enrichment analysis on differentially expressed genes relevant to hematopoiesis including many genes regarding the function of platelet/megakaryocyte (supplemental Figure 5D). These results indicated that mutated GNE influenced the expression of genes related to angiogenesis and platelet function. We performed reverse transcription quantitative real-time PCR (RT-qPCR; n = 3 in each group; primers are listed in supplemental Table 4) to validate the results of bulk RNA-seq (Figure 4C; Supplemental Table 5), and noted that several genes, especially *Esm1*, *Hk2*, and *Angpt2*, were differentially expressed ($P < .1$) between E11.5 wt/wt and mt/mt, which may explain the defective angiogenesis in embryonic development in mt/mt embryos.

Homozygous P735R mutation causes defective sialic acid biosynthesiss in mouse embryos

Western blotting analysis displayed greatly decreased intensity of the GNE protein band in mt/mt whole embryo lysates (Figure 5A), suggesting that *Gne* carrying P735R mutation causes impaired expression and/or stability of GNE protein. Lectin blotting of MAL-II, which binds to α-2,3 linked sialic acids, and peanut agglutinin (PNA), which preferentially binds to the de-sialylated core 1 *O*-glycan, as well as Sambucus nigra lectin, which binds to α-2,6 linked sialic acids, revealed that defective protein sialylation in mt/mt embryos relative to that of wt/wt (Figure 5C). Consistent with these lectin blotting results, PNA and MAL-II immunofluorescence staining revealed reduced sialylation in mt/mt brain tissue

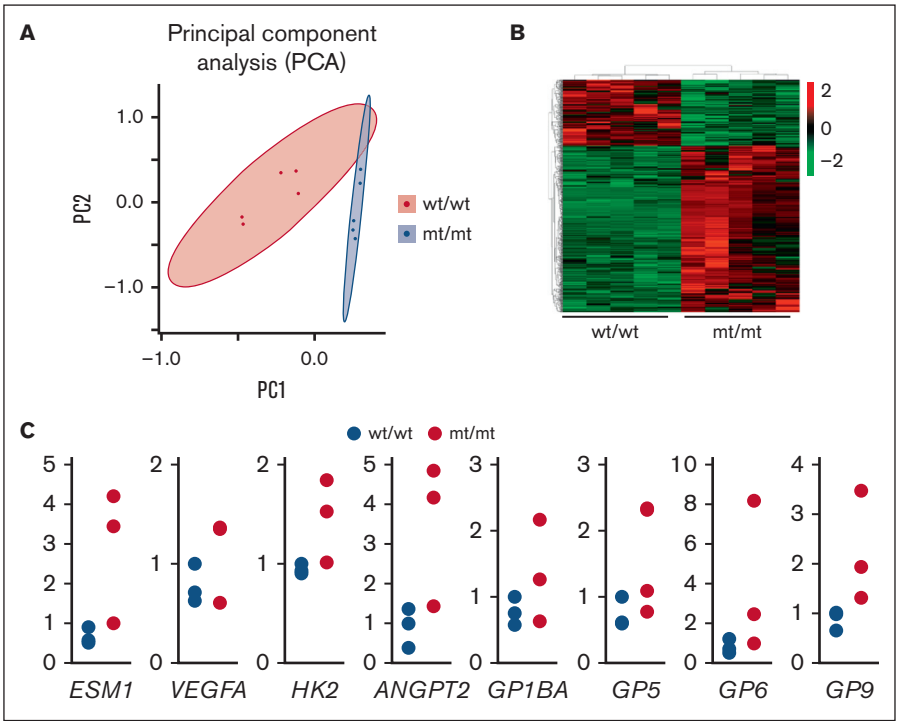

Figure 4. Bulk RNA sequencing of E11.5 embryos reveals significant differences in genome expression. (A) Principal component analysis displays the difference in global gene expression profiles between wt/wt and mt/mt embryos. N = 5 for each genotype. (B) Clustering analysis of differentially expressed genes of A shown as a heat map. (C) RT-qPCR of angiogenesis- and platelet-related differentially expressed genes scored by bulk RNA-seq. RNA was extracted from E11.5 embryonic heads. N = 3 for each genotype. All data were analyzed using *t*-tests.

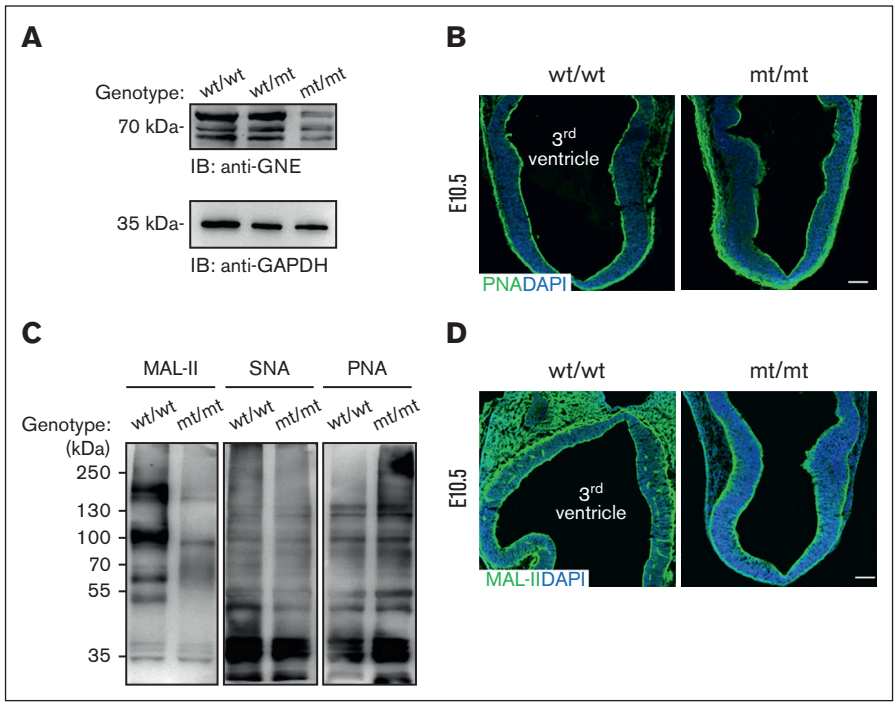

Figure 5. Homozygotic P735R mutation of *Gne* causes hyposialylation in mice. (A) Western blotting of GNE and GAPDH as loading control using mouse tissue extracts at E10.5. (B) Confocal images of PNA staining in wt/wt and mt/mt E10.5 embryos. (C) Lectin blotting of E10.5 tissue extracts probed with MAL-II, which detects α2,3-sialylated glycans, SNA, which detects α2,6-sialylated glycans, and PNA, which detects non-sialylated core 1 *O*-glycans (also known as T-antigen). The blots are representative of 4 independent experiments. (D) Confocal images of MAL-II staining in wt/wt and mt/mt E10.5 embryos. MAL-II, Maackia amurensis lectin II; PNA, peanut agglutinin. N = 3 for each genotype in (B) and (D). Scale bar, 100 μm.

compared with wt/wt brain tissue (Figure 5B,D). Of note, MAL-II strongly labeled angiogenic structures in the wt/wt brain tissue, implying a unique role for sialic acid in the developing vasculature.

Both patient-derived mutations impair de novo sialic acid biosynthesis

To determine the effects of both patient-derived mutations on the GNE function, a *Gne*-deficient (KO) MS1 mouse endothelial cell line was generated by CRISPR-Cas9 genome editing (Figure 6A). *Gne*-KO MS1 cells had reduced surface sialylation as revealed by a sialylation probe, SiaFind Lectenz, and increased exposure of desialylated glycans as shown by RCA1 staining, a probe for desialylated glycans (Figure 6B). To determine the specific role of each patient-derived GNE variant in sialylation, we transduced *Gne*-KO MS1 cells with lentiviral vectors encoding each patient-derived GNE with Flag3 tag (Figure 6C). Western blotting showed that the expression of wild-type (WT) GNE in transduced *Gne*-KO cells was similar to that in parental cells; however, the expression levels of both GNE variants were reduced (Figure 6D,F), which is consistent with the considerable reduction in the lysates from mt/mt mice, although the messenger RNA expression levels of *GNE* were equivalent among these transduced cells (supplemental Figure 6). *Gne*-KO MS1 cells transduced with WT but not the 2 GNE mutants normalized cell surface sialylation, indicating both mutations are loss of function (Figure 6E). Of note, cells transduced with C594Y-carrying GNE slightly restored cell surface sialylation with statistical significance (Figure 6E). This conclusion was further supported by normalizing SiaFind Lectenz binding with CD31 and VE-Cadherin expression, forward scatter, and GNE-Flag3 protein expression levels (supplemental Figure 7A-F). Given that residual expression of each GNE variant in transduced MS1 cells was detected, the dramatically reduced SiaFind Lectenz binding to cells expressing these GNE variants is presumably not due to reduced protein expression but impaired enzymatic activity of GNE. Immunocytochemical staining showed no difference among WT and 2 GNE mutants in their subcellular localization in the transduced MS1 cells (Figure 6F; supplemental Figure 8).

Both C594Y and P735R mutations are located on the kinase domain of GNE, thereby the kinase activity is most likely impaired in the patient. Furthermore, the kinase domain is required for the phosphorylation of ManNAc to ManNAc-6-phosphate during the de novo sialic acid biosynthetic pathway (Figure 6G). To investigate whether kinase function is impaired, *Gne*-KO MS1 cells transduced with each GNE variant were metabolically labeled with azide-labeled N-acetyl-mannosamine (ManNAz), and ManNAz-derived NeuAzylated glycans on the cell surface were examined by *Staudinger* ligation using a membrane-impermeable phosphine-biotin (Figure 6H). The results exhibited that NeuAz on the cell surface was increased in MS1 cells expressing WT GNE, whereas it was not observed in cells expressing each GNE variant. Taken together, these data demonstrated that both patient-derived GNE mutations are loss-of-function variants in de novo sialic acid biosynthesis, and P735R variant might be more pathogenic than C594Y variant.

To determine whether the reduced protein expression of cytosolic GNE carrying P735R was due to accelerated protein degradation through the ubiquitin-proteasome pathway, MS1 cells with WT or P735R-carrying GNE were pretreated with MG132, a proteasome inhibitor. However, GNE protein expression in cell lysates and the level of poly-ubiquitinated GNE among these transduced cells were not affected by proteasome inhibition, suggesting that the ubiquitin-proteasome pathway does not contribute to the reduced protein expression of GNE carrying P735R (supplemental Figure 9A-C). In a previous report, GNE mutations may cause alterations in the actin cytoskeleton that affect cell dynamics.[23] To test this, actin cytoskeleton and microtubules were analyzed in

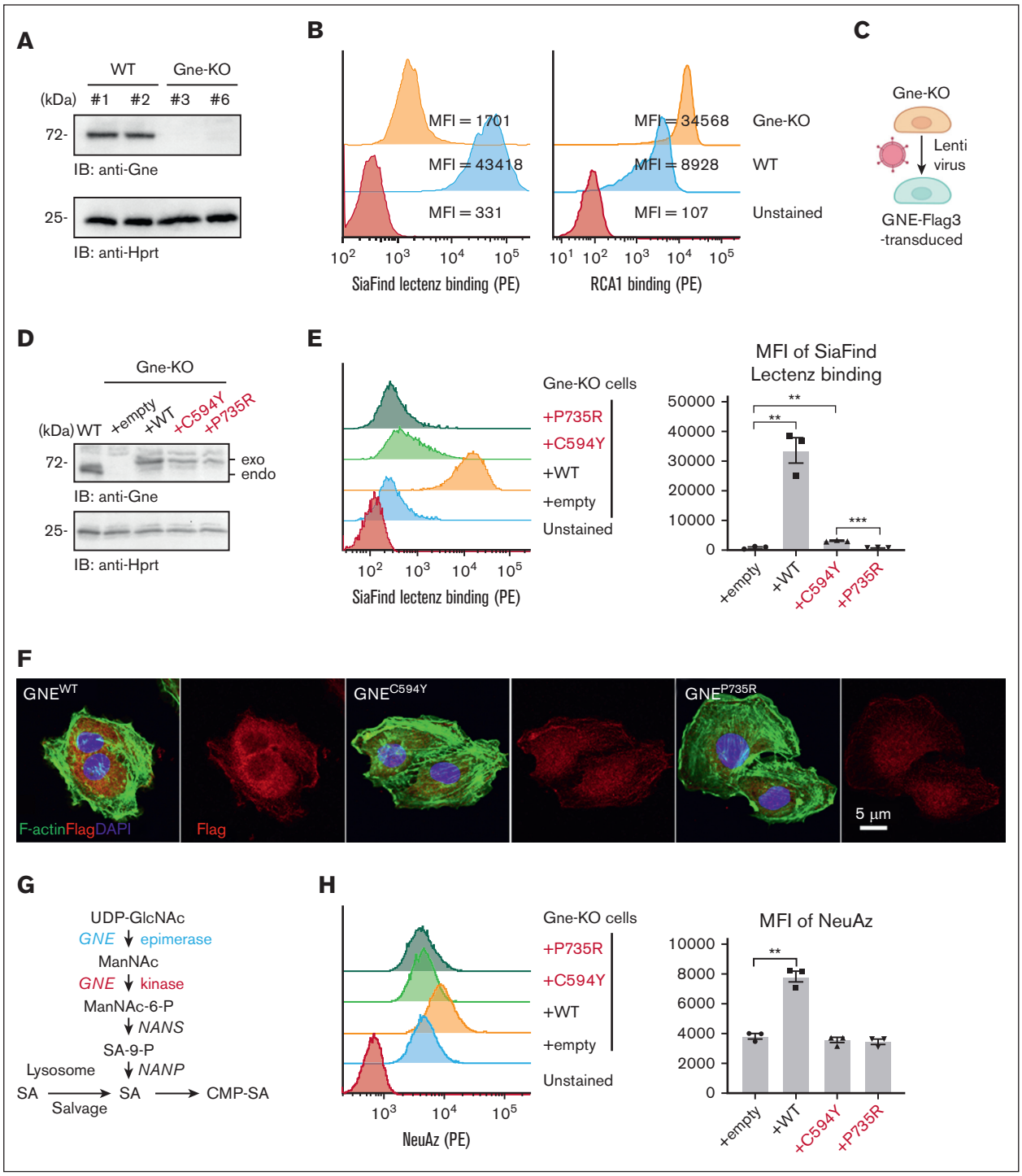

Figure 6. Both patient-derived GNE mutations severely affect de novo sialic acid biosynthesis. (A) Establishment of *Gne*-knockout mouse endothelial cell line MS1 validated by western blotting. Hprt, housekeeping protein. (B) Altered glycans on the cell surface of *Gne*-KO MS1 cells examined by flow cytometry using SiaFind Lectenz (pan-sialic acid probe) and RCA1 lectin (asialylated glycan lectin). The unstained control was used as a negative control. (C) *Gne*-KO MS1 cells were lentivirally infected with empty control or each GNE-Flag3 variant. (D) Expression analysis of each GNE protein by western blotting. Exogenously transduced GNE (exo) and endogenous Gne (endo) are distinguished by size based on Flag3 tag on transduced GNE. WT, wild type. (E) Infected cells were analyzed for SiaFind Lectenz binding by flow cytometry. (F) Expression of cytoplasmic GNE was reduced in MS1 cells transduced with mutant GNE imaged by confocal microscopy. Flag3, Flag3-tagged GNE; DAPI, nuclear marker. (G) Two pathways of sialic acid biosynthesis. (H) ManNAz-derived NeuAz on cell surface glycans of cells that were metabolically labeled with ManNAz for 3 days. $^{**}P < .01$; $^{***}P < .001$.

Gne-KO MS1 cells, but none of them showed altered distribution and expression (supplemental Figure 10).

Discussion

In this article, we report a macrothrombocytopenia patient without myopathy carrying compound heterozygous *GNE* missense variants, c.1781G>A and c.2204C>G, both of which are novel. We simulated how 2 mutations influence protein structure respectively and found that P735R is more likely to damage the steric stabilization of GNE, indicating P735R might be more pathogenic; thus, we generated a new mouse model carrying the c.2204C>G (p.P735R) variant in both alleles. Unexpectedly, mt/mt embryos died before E12.5, resembling global Gne-KO mice,[24] and exhibited a brain bleeding phenotype similar to *T-syn*$^{-/-}$ mice.[25]

T-synthase (T-syn) is a glycosyltransferase that transfers galactose from UDP-galactose on N-acetylgalactosamine α1-serine/threonine (Tn antigen) on carrier proteins to form galactose β1-3 N-acetylgalactosamine α1-serine/threonine (T antigen or core 1 *O*-glycan). Core 1 *O*-glycan is commonly capped by sialic acids. Sialylated T antigen is expressed primarily on endothelial, hematopoietic, and epithelial cells during mouse development. We have previously reported that global *T-syn*$^{-/-}$ mice fail to produce sialylated T antigen, and progressively develop lethal cerebrospinal hemorrhage from E11, similar to our mt/mt mice.[25] Our recent study has shown that podoplanin (Pdpn), a highly sialylated core 1 *O*-glycoprotein expressed on neuroepithelial cells, is critically involved in embryonic vascular integrity via interaction with platelet Clec-2.[22] Mice lacking either Pdpn or Clec-2 also develop cerebrospinal hemorrhage phenotypes preceded by abnormal angiogenic sprouting that are similar to those of global *T-syn*$^{-/-}$ and mt/mt mice. These data strongly suggest that hemorrhages and abnormal angiogenesis in mt/mt mice are caused, in part, by the impaired function of sialylated core 1 *O*-glycoproteins such as podoplanin.

Interestingly, mouse models carrying other *Gne* missense mutations can live for several days or even longer after birth, and have renal failure syndrome and myopathy.[26-29] To some extent, this phenotypic heterogeneity of *Gne* mutants in mice corroborates the very essence that different *GNE* mutations cause different types of disease in humans. Given that our mt/mt embryos are embryonic lethal, the residual activity in GNE carrying C594Y in our patient shown in Figure 6E is most likely critical for survival. Thus, we expect that mice carrying homozygous C594Y will show prolonged survival and enable us to study the mechanism of macrothrombocytopenia in postnatal stages as an appropriate patient model, which will be our future direction.

GNE is the key rate-limiting enzyme in the sialic acid synthesis pathway, and thus current hypotheses about the pathological GNE pathway mostly focus on the sialylation defect of glycans.[18,19,26,30] α-Dystroglycan (α-DG), an extracellular domain of dystroglycan, functions in skeletal muscle as a receptor for extracellular matrices (ECMs) such as laminin, agrin, and perlecan, and transduces external ECM signals into the actin cytoskeleton. The interaction of α-DG with ECMs depends on a unique glycosylation displayed on *O*-mannosylated glycan (ie, phospho-core M3 structure with repetitive disaccharides consisting of glucuronic acid and xylose). A possible mechanistic insight into GNE myopathy is based on the defective binding of laminin to α-dystroglycan of *Gne* mutants.[10] These data suggest that GNE is directly or indirectly involved in the generation of a functional laminin-binding epitope of glycans on α-dystroglycan. Congenital disorders of glycosylation (CDGs) are a large diverse disease group of approximately 170 rare inherited glycosylation-defective disorders.[31,32] When it comes to CDG-II (ie, disorders affecting glycan composition), it is quite rare compared to CDG-I, and accounts for only 6% of all CDGs.[33] *GNE* is scored as one of such CDG-II causative genes. *SLC35A1* is a sole CMP-sialic acid transporter in the Golgi. CDG-IIf caused by *SLC35A1* mutations develop platelet abnormality just like *GNE* mutations.[34] Interestingly, phenotypes in *GNE* and *SLC35A1* variants in humans share similar platelet and skeletal muscle phenotypes. This is because *SLC35A1* also functions as sole CDP-ribitol transporter in the Golgi that is essential for matriglycan formation on α-DG.[35,36] Along the these lines, other investigators hold the views that GNE mutation disrupts the distribution of actin, a cytoskeletal protein.[23,37] The *GNE*-KO zebrafish model also displayed skeletal muscle defects.[38] Oral sugar supplementation, such as mannosamine (ManN), N-acetylmannosamine (ManNAc), and N-glycolylneuraminic acid (Neu5Gc) as external sources of free sialic acid, has been proposed to bypass GNE dysfunction for the treatment of sialylation impairment in vivo.[39-41] A phase 2 clinical trial demonstrated the efficacy of oral ManNAc in GNE myopathy patients.[42] Recently, Crowe et al developed a recombinant adeno associated virus (rAAV) vector with a muscle-specific promoter-driven GNE expression cassette in transgenic mice carrying the myopathogenic D207V mutation in *Gne* together with oral administration of NeuGc, and observed a significant increase in Neu5Gc immunostaining in muscle, suggesting the potential of gene therapy in the treatment of *GNE*-related diseases.[41] We also investigated how Gne variants affect de novo sialic acid biosynthesis using ManNAz, and found that ManNAz-derived NeuAz on the cell surface was lower in MS1 cells expressing both GNE variants than in cells expressing wild-type GNE, demonstrating that compromised de novo sialic acid biosynthesis in the patient results from loss of function of GNE protein, especially in kinase activity.

In our study, the early embryonic lethality of mt/mt mice prevented us from investigating whether thrombogenesis and skeletal muscle functions are impaired in mt/mt mice as observed in patients with GNE. Nevertheless, our study reveals a novel role of GNE in angiogenesis during embryonic development. Recently, we have reported that deletion of a CMP-sialic acid transporter (Slc35a1), which leads to a complete loss of sialylation, specifically in platelets/megakaryocytes in mice, results in macrothrombocytopenia.[34] Thus, the macrothrombocytopenic phenotype in our patient is presumably caused by limited bioavailability of sialic acid in megakaryocytes and platelets. Besides, eMKs and platelets are indispensable for maintaining the structure of the vasculature, and we observed that the count of circulating eMKs and platelets was significantly decreased, while plenty of eMKs were abnormally accumulated in the vasculature in mt/mt embryonic brains, which is similar to the phenotypes of the *T-syn*$^{-/-}$, *Pdpn*$^{-/-}$ and *Clec-2*$^{-/-}$ embryos.[22] Recently, an association study of SNPs and platelet counts has been published. The meta-GWAS analysis of platelet counts using data from 536 974 Europeans identified 577 variants.[43] However, GNE gene was not found in the variant list, which may be due to the extreme rarity of GNE variants in the data used. The molecular mechanisms underlying GNE in angiogenesis also remain to be determined, and whether GNE regulates vascular development by influencing eMKs or other growth factors such as angiopoietin-2 (Angpt2) would be an interesting direction for future studies. Our bulk RNA-seq data

revealed differentially expressed genes mainly involved in angiogenesis and platelet functions in E11.5 mt/mt embryos compared to wild-type embryos. Unexpectedly, we also found altered sugar metabolism (related to energy production). Interestingly, this is partially consistent with the finding of altered skeletal muscle protein composition in patients with GNE myopathy.[44]

In summary, our data demonstrate that novel missense variants of *GNE* cause macrothrombocytopenia in human and embryonic lethality in mouse development. Importantly, this study provides insights into the unexpected function of GNE in angiogenesis. Our findings may lead to new insights and novel treatments for these GNE-related diseases.

Acknowledgments

This work was supported by funds from the Jiangsu Provincial Key Medical Center (YXZXA2016002), the Priority Academic Program Development of Jiangsu Higher Education Institutions, and iGCORE Open Collaborative Research 2022.

Authorship

Contribution: L.H., Y.K., C.R., and L.X. conceived and designed research; L.H., Y.K., L.C., J.H., B.Z., F.Y., Y.L., Z.M., T.L., X.B., and M.J. performed the experiments and analyzed data; C.R. provided funding; and L.H., Y.K., and L.X. interpreted the data and wrote the manuscript.

Conflict-of-interest disclosure: The authors declare no competing financial interests.

ORCID profiles: L.H., 0009-0007-5709-6874; B.Z., 0000-0002-4104-7281; Y.L., 0000-0002-0990-5338; L.X., 0000-0002-9586-7971.

Correspondence: Lijun Xia, Cardiovascular Biology Research Program, Oklahoma Medical Research Foundation, 825 NE 13th St, Oklahoma City, OK 73104; email: Lijun-xia@omrf.org; and Changgeng Ruan, The First Affiliated Hospital of Soochow University, 188 Shizi St, Suzhou, 215006, China; email: ruanchanggeng@suda.edu.cn.

References

1. Macauley MS, Crocker PR, Paulson JC. Siglec-mediated regulation of immune cell function in disease. *Nat Rev Immunol*. 2014;14(10):653-666.
2. Smith BAH, Bertozzi CR. The clinical impact of glycobiology: targeting selectins, Siglecs and mammalian glycans. *Nat Rev Drug Discov*. 2021;20(3):217-243.
3. Li Y, Chen X. Sialic acid metabolism and sialyltransferases: natural functions and applications. *Appl Microbiol Biotechnol*. 2012;94(4):887-905.
4. Hinderlich S, Stäsche R, Zeitler R, Reutter W. A bifunctional enzyme catalyzes the first two steps in N- acetylneuraminic acid biosynthesis of rat liver. Purification and characterization of UDP-N-acetylglucosamine 2-epimerase/N-acetylmannosamine kinase. *J Biol Chem*. 1997;272(39):24313-24318.
5. Tanner ME. The enzymes of sialic acid biosynthesis. *Bioorg Chem*. 2005;33(3):216-228.
6. Seppala R, Lehto VP, Gahl WA. Mutations in the human UDP-N-acetylglucosamine 2-epimerase gene define the disease sialuria and the allosteric site of the enzyme. *Am J Hum Genet*. 1999;64(6):1563-1569.
7. Celeste FV, Vilboux T, Ciccone C, et al. Mutation update for *GNE* gene variants associated with GNE myopathy. *Hum Mutat*. 2014;35(8):915-926.
8. Krasnewich DM, Tietze F, Krause W, et al. Clinical and biochemical studies in an American child with sialuria. *Biochem Med Metab Biol*. 1993;49(1):90-96.
9. Eisenberg I, Avidan N, Potikha T, et al. The UDP-N-acetylglucosamine 2-epimerase/N-acetylmannosamine kinase gene is mutated in recessive hereditary inclusion body myopathy. *Nat Genet*. 2001;29(1):83-87.
10. Huizing M, Rakocevic G, Sparks SE, et al. Hypoglycosylation of α-dystroglycan in patients with hereditary IBM due to GNE mutations. *Mol Genet Metab*. 2004;81(3):196-202.
11. Tajima Y, Uyama E, Go S, et al. Distal myopathy with rimmed vacuoles: Impaired O-glycan formation in muscular glycoproteins. *Am J Pathol*. 2005;166(4):1121-1130.
12. Endo T. Glycobiology of α-dystroglycan and muscular dystrophy. *J Biochem*. 2015;157(1):1-12.
13. Weiss P, Tietze F, Gahl WA, Seppala R, Ashwell G. Identification of the metabolic defect in sialuria. *J Biol Chem*. 1989;264(30):17635-17636.
14. Murtazina A, Nikitin S, Rudenskaya G, et al. Genetic and clinical spectrum of GNE myopathy in Russia. *Genes*. 2022;13(11):1991.
15. Manchev VT, Hilpert M, Berrou E, et al. A new form of macrothrombocytopenia induced by a germ-line mutation in the PRKACG gene. *Blood*. 2014;124(16):2554-2563.
16. Revel-Vilk S, Shai E, Turro E, et al. GNE variants causing autosomal recessive macrothrombocytopenia without associated muscle wasting. *Blood*. 2018;132(17):1851-1854.
17. Futterer J, Dalby A, Lowe GC, et al. Mutation in GNE is associated with severe congenital thrombocytopenia. *Blood*. 2018;132(17):1855-1858.
18. Zieger B, Boeckelmann D, Anani W, et al. Novel GNE gene variants associated with severe congenital thrombocytopenia and platelet sialylation defect. *Thromb Haemost*. 2022;122(7):1139-1146.
19. Smolag KI, Fager Ferrari M, Zetterberg E, et al. Severe congenital thrombocytopenia characterized by decreased platelet sialylation and moderate complement activation caused by novel compound heterozygous variants in GNE. *Front Immunol*. 2021;12:777402.
20. Li H, Ji CY, Zong XN, Zhang YQ. [Height and weight standardized growth charts for Chinese children and adolescents aged 0 to 18 years]. *Zhonghua Er Ke Za Zhi*. 2009;47(7):487-492.

21. Li Y, Fu J, Ling Y, et al. Sialylation on O-glycans protects platelets from clearance by liver Kupffer cells. *Proc Natl Acad Sci U S A*. 2017;114(31):8360-8365.
22. Hoover C, Kondo Y, Shao B, et al. Heightened activation of embryonic megakaryocytes causes aneurysms in the developing brain of mice lacking podoplanin. *Blood*. 2021;137(20):2756-2769.
23. Devi SS, Yadav R, Arya R. Altered actin dynamics in cell migration of GNE mutant cells. *Front Cell Dev Biol*. 2021;9:603742.
24. Wedekind H, Kats E, Weiss AC, et al. *Uridine diphosphate-N-acetylglucosamine-2-epimerase/N-acetylmannosamine kinase* deletion in mice leads to lethal intracerebral hemorrhage during embryonic development. *Glycobiology*. 2021;31(11):1478-1489.
25. Xia L, Ju T, Westmuckett A, et al. Defective angiogenesis and fatal embryonic hemorrhage in mice lacking core 1–derived O-glycans. *J Cell Biol*. 2004;164(3):451-459.
26. Galeano B, Klootwijk R, Manoli I, et al. Mutation in the key enzyme of sialic acid biosynthesis causes severe glomerular proteinuria and is rescued by N-acetylmannosamine. *J Clin Invest*. 2007;117(6):1585-1594.
27. Malicdan MCV, Noguchi S, Nonaka I, Hayashi YK, Nishino I. A Gne knockout mouse expressing human GNE D176V mutation develops features similar to distal myopathy with rimmed vacuoles or hereditary inclusion body myopathy. *Hum Mol Genet*. 2007;16(22):2669-2682.
28. Ito M, Sugihara K, Asaka T, et al. Glycoprotein hyposialylation gives rise to a nephrotic-like syndrome that is prevented by sialic acid administration in GNE V572L point-mutant mice. Akagi T, ed. *PLoS One*. 2012;7(1):e29873.
29. Sela I, Yakovlev L, Becker Cohen M, et al. Variable phenotypes of knockin mice carrying the M712T gne mutation. *Neuromol Med*. 2013;15(1):180-191.
30. Noordermeer T, van Asten I, Schutgens REG, et al. Enhanced hepatic clearance of hyposialylated platelets explains thrombocytopenia in GNE-related macrothrombocytopenia. *Blood Adv*. 2022;6(11):3347-3351.
31. Ng BG, Freeze HH. Perspectives on glycosylation and its congenital disorders. *Trends Genet*. 2018;34(6):466-476.
32. CDG Hub. Accessed 13 October 2023. https://www.cdghub.com
33. Pascreau T, Auditeau C, Borgel D. Hemostatic defects in congenital disorders of glycosylation. *Res Pract Thromb Haemost*. 2023;7(3):100142.
34. Ma X, Li Y, Kondo Y, et al. Slc35a1 deficiency causes thrombocytopenia due to impaired megakaryocytopoiesis and excessive platelet clearance in the liver. *Haematol*. 2021;106(3):759-769.
35. Riemersma M, Sandrock J, Boltje TJ, et al. Disease mutations in CMP-sialic acid transporter SLC35A1 result in abnormal -dystroglycan O-mannosylation, independent from sialic acid. *Hum Mol Genet*. 2015;24(8):2241-2246.
36. Ury B, Potelle S, Caligiore F, Whorton MR, Bommer GT. The promiscuous binding pocket of SLC35A1 ensures redundant transport of CDP-ribitol to the Golgi. *J Biol Chem*. 2021;296:100789.
37. Harazi A, Becker-Cohen M, Zer H, Moshel O, Hinderlich S, Mitrani-Rosenbaum S. The interaction of UDP-N-acetylglucosamine 2-epimerase/N-acetylmannosamine Kinase (GNE) and Alpha-Actinin 2 is altered in GNE myopathy M743T mutant. *Mol Neurobiol*. 2017;54(4):2928-2938.
38. Livne H, Avital T, Ruppo S, Harazi A, Mitrani-Rosenbaum S, Daya A. Generation and characterization of a novel gne Knockout Model in Zebrafish. *Front Cell Dev Biol*. 2022;10:976111.
39. Niethamer TK, Yardeni T, Leoyklang P, et al. Oral monosaccharide therapies to reverse renal and muscle hyposialylation in a mouse model of GNE myopathy. *Mol Genet Metabol*. 2012;107(4):748-755.
40. Xu X, Wang AQ, Latham LL, et al. Safety, pharmacokinetics and sialic acid production after oral administration of N -acetylmannosamine (ManNAc) to subjects with GNE myopathy. *Mol Genet Metabol*. 2017;122(1-2):126-134.
41. Crowe KE, Zygmunt DA, Heller K, et al. Visualizing muscle sialic acid expression in the GNED207VTgGne-/- Cmah-/- Model of GNE myopathy: a comparison of dietary and gene therapy approaches. *JND*. 2022;9(1):53-71.
42. Carrillo N, Malicdan MC, Leoyklang P, et al. Safety and efficacy of N-acetylmannosamine (ManNAc) in patients with GNE myopathy: an open-label phase 2 study. *Genet Med*. 2021;23(11):2067-2075.
43. Mikaelsdottir E, Thorleifsson G, Stefansdottir L, et al. Genetic variants associated with platelet count are predictive of human disease and physiological markers. *Commun Biol*. 2021;4(1):1132.
44. Cho A, Christine M, Malicdan V, et al. Sialic acid deficiency is associated with oxidative stress leading to muscle atrophy and weakness in GNE myopathy. *Hum Mol Genet*. 2017;26(16):3081-3093.